UDC 621.3 https://doi.org/10.20998/2074-272X.2022.2.10

T. Praveen Kumar, S. Ganapathy, M. Manikandan

Improvement of voltage stability for grid connected solar photovoltaic systems using static synchronous compensator with recurrent neural network

Purpose. *This article proposes a new control strategy for static synchronous compensator in utility grid system. The proposed photovoltaic fed static synchronous compensator is utilized along with recurrent neural network based reference voltage generation is presented in grid system network.* ***The novelty*** *of the proposed work consists in presenting a Landsman converter enhanced photovoltaic fed static synchronous compensator with recurrent neural network algorithm, to generate voltage and maintain the voltage-gain ratio.* ***Methods.*** *The proposed algorithm which provides sophisticated and cost-effective solution for utilization of adaptive neuro-fuzzy inference system as maximum power point tracking assures controlled output and supports the extraction of complete power from the photovoltaic panel. Grid is interconnected with solar power, voltage phase angle mismatch, harmonic and voltage instability may occur in the distribution grid. The proposed control technique strategy is validated using MATLAB/Simulink software and hardware model to analysis the working performances.* ***Results.*** *The results obtained show that the power quality issue, the proposed system to overcome through elimination of harmonics, reference current generation is necessary, which is accomplished by recurrent neural network. By recurrent neural network, the reference signal is generated more accurately and accordingly the pulses are generated for controlling the inverter.* ***Originality.*** *Compensation of power quality issues, grid stability and harmonic reduction in distribution network by using photovoltaic fed static synchronous compensator is utilized along with recurrent neural network controller.* ***Practical value****. The work concerns the comparative study and the application of static synchronous compensator with recurrent neural network controller to achieve a good performance control system of the distribution network system. This article presents a comparative study between the conventional static synchronous compensator, static synchronous compensator with recurrent neural network and hardware implementation with different load. The strategy based on the use of a static synchronous compensator with recurrent neural network algorithm for the control of the continuous voltage stability and harmonic for the distribution network-linear as well as non-linear loads in efficient manner. The study is validated by the simulation results based on MATLAB/Simulink software and hardware model.* References 29, tables 2, figures 25.

Key words: **static synchronous compensator, photovoltaic fed, adaptive neuro-fuzzy inference system, recurrent neural network.**

Мета*. У статті пропонується нова стратегія управління статичним синхронним компенсатором в енергосистемі. Запропонований статичний синхронний компенсатор з живленням від фотоелектричних елементів використовується разом з генератором опорної напруги на основі нейронної рекурентної мережі, представленим в мережі енергосистеми.* ***Новизна*** *запропонованої роботи полягає у поданні статичного синхронного компенсатора з покращеним фотоелектричним перетворювачем Ландсмана з алгоритмом рекурентної нейронної мережі для генерації напруги та підтримки коефіцієнта посилення за напругою.* ***Методи****. Запропонований алгоритм, який забезпечує ефективне та економічне рішення для використання адаптивної нейро-нечіткої системи логічного виведення як відстеження точки максимальної потужності, забезпечує контрольований вихід та підтримує вилучення повної потужності з фотогальванічної панелі. Мережа взаємопов'язана із сонячною енергією, у розподільній мережі можуть виникати невідповідність фазового кута напруги, гармоніки та нестабільність напруги. Запропонована стратегія методу управління перевіряється з використанням моделей програмного забезпечення MATLAB/Simulink та апаратного забезпечення для аналізу робочих характеристик.* ***Результати****. Отримані результати показують, що проблема якості електроенергії, яку запропонована система долає за допомогою усунення гармонік,потребує генерації еталонного струму, що здійснюється рекурентною нейронної мережею. За допомогою рекурентної нейронної мережі більш точно формується еталонний сигнал і відповідно генеруються імпульси для керування інвертором.* ***Оригінальність****. Компенсація проблем з якістю електроенергії, стабільністю мережі та зниженням гармонік у розподільній мережі за допомогою статичного синхронного компенсатора з фотоелектричним живленням використовується разом із контролером рекурентної нейронної мережі.* ***Практична цінність****. Робота стосується порівняльного дослідження та застосування статичного синхронного компенсатора з рекурентним нейромережевим контролером для досягнення хорошої продуктивності системи управління системою розподільної мережі. У цій статті представлено порівняльне дослідження традиційного статичного синхронного компенсатора, статичного синхронного компенсатора з рекурентною нейронною мережею та апаратною реалізацією з різним навантаженням. Стратегія, що ґрунтується на використанні статичного синхронного компенсатора з рекурентним алгоритмом нейронної мережі для ефективного контролю стабільності постійної напруги та гармонік для лінійних та нелінійних навантажень розподільної мережі. Дослідження підтверджується результатами моделювання з урахуванням програмно-апаратної моделі MATLAB/Simulink..* Бібл. 29, табл. 2, рис. 25.

Ключові слова: **статичний синхронний компенсатор, фотоелектричне живлення, адаптивна нейро-нечітка система виведення, рекурентна нейронна мережа.**

Abbreviations

ANFIS	Adaptive Neuro-Fuzzy Inference System	PI	Proportional-Integral
ANN	Artificial Neural Network	P-O	Perturb-Observe
DVR	Dynamic Voltage Restorer	PV	Photovoltaic
FACTS	Flexible AC Transmission System	RNN	Recurrent Neural Network
FFT	Fast Fourier Transform	SEPIC	Single Ended Primary Inductance Converter
FIS	Fuzzy Inference System	SRF	Synchronous Reference Frame
IC	Incremental Conductance	STATCOM	Static Synchronous Compensator
LSTM	Long Short-Term Memory	THD	Total Harmonic Distortions
MPPT	Maximum Power Point Tracking	VSI	Voltage Source Inverter
PCC	Point of Common Coupling		

Introduction. Nowadays, power quality is considered as a major issue in industrial sectors because of increasing sensitive loads [1, 2]. In general, the power quality problems greatly affect the distribution side which results in malfunctioning and failure of sensitive loads

© T. Praveen Kumar, S. Ganapathy, M. Manikandan

[3]. Majority of power quality issues are caused by non-linear loads and harmonic imbalances [4]. Voltage sag/swell, harmonic distortions, spikes and surges and transient disruptions are the most serious power quality issues that severely affect the power distribution system [5, 6]. Thus in modern power systems, stability enhancement and reactive power compensation are the important actualities; DVR, a FACTS device is widely employed in achieving so. It solves the voltage sag problem in a unique way, however, it only compensates for a specific proportion of sag, and so the power quality problem is not totally eliminated [7-9].

Therefore, one of the excellent FACTS device called STATCOM is utilized in this work which assists in improvising the sag/ swell control, dynamic voltage control, real and reactive power control etc., providing better power quality and voltage stability [10-12]. Due to advanced technologies including incorporation of large-scale renewable distributed generation, enhanced communication as well as control methods, and increased storage capacity, generation of power and distribution networks are facing significant variations. Owing to the static structure, minimal size, and low cost for maintenance, solar PV dependent energy generation systems are widely used by various renewable resources for the generation of power [13]. Since solar PV energy is intermittent, the PV systems are combined with storage systems for energy as well as other sources for renewable energy to ensure trustworthy functioning. This is attained by the parallel connection of DC-DC converters with PV panel [14]. A DC-DC converter is necessary amidst the inverter and the PV panel for avoiding large number of PV panels connected in series manner. This converter is also essential in power generation of PV system for providing electrical isolation [15].

Regarding DC-DC converters, boost converters are used in increasing the PV panel voltage and their incorporation reduces the input ripple current obtained from the solar panel, increasing the panel's reliability and extraction power [16]. Despite these benefits, boost converters have a discontinuous input and output, necessitating a greater number of switching devices. This influences the circuit dynamics by causing fluctuations in the gain of the circuit [17]. To overcome this limitation, a buck-boost converter has been developed, which has a wide input and output voltage range with increased performance. It achieves an additional input feature that increases the dc input voltage range, greatly improving the PV panel's versatility but possesses centralized operation [18]. Zeta converter is also utilized in PV systems which generate minimal ripple current and improved voltage gain but the gain of voltage is sensible with the inductance leakage [19]. CUK converters employed by the PV panel exhibited minimal switching losses together with better voltage regulation and greater efficiency providing versatile operation. However, due to the resulting sharp speed up/down voltage, these converters lagged, impacting the precise utilization [20]. Furthermore, CUK converter utilization is restricted to the medium-low power range, as high-power operation necessitates large input and output inductors, and the converter is harmed when linked to a utility grid due to grid voltage fluctuations [21, 22]. Moreover, SEPIC converters are utilized in PV systems to generate an output which is non-inverting and is considered as easy to drive due to the referenced switch towards ground node. However, these converters are not finer in terms of cost and efficiency [23]. In order to tackle these issues, Landsman converter is exploited which offers noiseless operation with improved efficiency.

To extract the full quantity of solar power, the DC-DC converter is used in conjunction with a MPPT controller. It is a significant component included in PV systems to improve the efficiency of extracting renewable energy. Numerous schemes for MPPT control are proposed and in most of them, PV voltage is selected as the variable for control because of its enhanced characteristics for stability [24]. P-O is a commonly used MPPT algorithm because of its simplicity and cost-effectiveness. The perturbation's phase size is estimated by the tradeoff amidst MPPT precision and MPPT rate which is little tedious. The use of IC instead of P-O, which is free of oscillations while tracking the maximum power point, yields more precise performance. Despite these benefits, this approach is limited by environmental conditions [25]. These flaws are overcome by employing closed loop control algorithms that balance the DC-link voltages, resulting in minimal distortions and efficiently preserving the grid system's power quality [26]. Closed loop algorithms produce optimal results when dealing with external disruptions, allowing grids to operate in real time but result in high emission costs due to less emission allowance [27]. To overcome these issues, ANFIS is exploited in this approach which combines the benefits of complementary ANN and fuzzy logic algorithms, resulting in better fuzzy controller accuracy and a shorter development time.

Furthermore, the converter's output DC voltage is transformed to AC voltage, which is accomplished by a 3ϕ VSI that is grid connected. The synchronization of grid is regarded as a significant challenge due to issues such as voltage distortions induced by local nonlinear loads and grid disturbances. The basic elements of the common coupling voltage point are evaluated with the consideration of power quality variations for achieving improved synchronization of grid [28, 29]. These grid synchronization frameworks improve control efficiency and interpolate improved grid quality power, resulting in precise outcomes. The control architectures considered are complex hybrid systems that combine classical and modern techniques, such as artificial intelligence and statistical models.

The **goal** of this paper is the synthesis of a recurrent neural network based reference current generation control structure and the identification of the latest trends. The main findings are summarized in the development of increasingly robust controllers for operation with improved efficiency, power quality, stability, safety, and economics. A Landsman converter is exploited which acts as a ripple filter and boosts the oscillating PV voltage. An MPPT controller adopting ANFIS is utilized for providing better accuracy. RNN based reference current generation is utilized for effective harmonic elimination. A 3ϕ VSI for inverting the input DC voltage along with LC filter and AC grid is also employed in STATCOM applications.

Proposed control system. The schematic diagram for the proposed approach is given in Fig. 1, in which the

voltage stability of the power system is enhanced by the implementation of STATCOM. PV power is applied to the STATCOM along a Landsman converter. The point of functioning of PV array is at the maximum power point while the converter power is grid synchronized. For the controlling of Landsman converter, an MPPT controller is connected which tracks the maximum power by evaluating the current as well as voltage obtained from the PV array. It regulates the reference voltage or duty cycle for matching the power to instant power point. The MPPT controller exploits ANFIS and is non-linear and varies in accordance with time. It performs the evaluation of signals and its optimal selection thus mitigating the steady-state error.

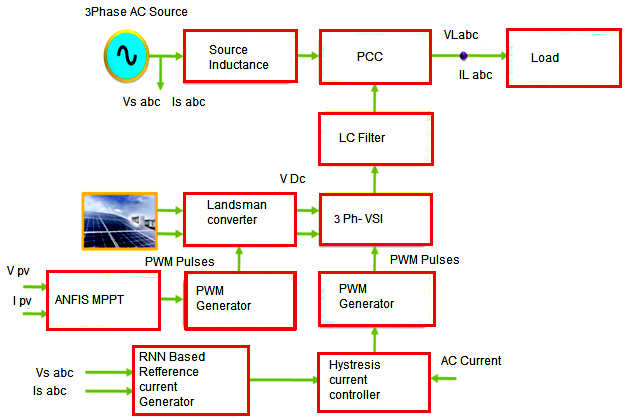

Fig. 1. Schematic diagram of the proposed approach

RNN based reference current generation is utilized in this work, by which the harmonics are eliminated for any change in load and source voltage. Thus, the pulses for controlling the VSI are generated by using hysteresis current controller, thereby providing reactive power compensation and harmonic elimination.

Modeling of PV system. A solar cell is essentially a semiconductor diode that is exposed to irradiance. This solar irradiance comprises of photons having various levels of energy of which few are absorbed in *p-n* junction. The photons with minimum energy level when compared to the solar cell's band gap are unusable. The photons with maximum energy when compared to band gap are utilized in the range similar to band gap. The equivalent circuits generally utilized for the PV cell modeling consists of a single diode offering better tradeoff between simplicity and accuracy and the corresponding diagram is shown in Fig. 2.

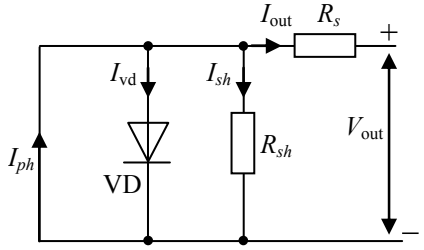

Fig. 2. Equivalent circuit of PV cell

The photo current I_{ph} is based on the solar radiation R and temperature T and is given by

$$I_{ph} = I_{ph}(T_{ref}) \cdot \left(1 + k_0 \cdot (T - T_{ref})\right); \quad (1)$$

$$I_{ph}(T_{ref}) = \frac{R}{R_{ref}} \cdot I_{sc}(T_{ref}), \quad (2)$$

where $I_{ph}(T_{ref})$ is the photo current corresponding to nominal temperature T_{ref}; R_{ref} is the radiation which is nominal obtained by PV's constructor; k_0 is the constant which is given as

$$k_0 = \frac{I_{sc}(T) - I_{sc}(T_{ref})}{T - T_{ref}}, \quad (3)$$

where I_{sc} is the current across short circuit.

In PV system, the temperature of environment is a nominal one and from (1), (2) for $T = T_{ref}$, the photo current I_{ph} depends on solar radiation and is given as

$$I_{ph} = I_{ph}(T_{ref}) = \frac{R}{R_{ref}} \cdot I_{sc}(T_{ref}). \quad (4)$$

Equation (5) denotes diode equation in which V_{out} and I_{out} are the current as well as voltage outputs, I_{sat} is the saturation current of the diode VD, V_{th} is the thermal voltage of the diode, R_s is the resistance in series

$$I_d = I_{sat}\left[\exp\left(\frac{V_{out} + I_{out} \cdot R_s}{V_{th}}\right) - 1\right]. \quad (5)$$

The current across parallel resistance is given as

$$I_{sh} = \frac{V_{out} + I_{out} \cdot R_s}{R_{sh}}. \quad (6)$$

The V-I characteristic equation is given as

$$I_{out} = I_{ph} - I_{sat}\left[\exp\left(\frac{V_{out} + I_{out} \cdot R_s}{V_{th}}\right) - 1\right] - \left(\frac{V_{out} + I_{out} \cdot R_s}{R_{sh}}\right). \quad (7)$$

Thus, the modeling of PV system is performed and from (7), the output voltage and the input voltage are evaluated.

Modeling of Landsman converter. Landsman converter is a DC-DC converter which is used to enhance the voltage attained from the PV system providing a noiseless operation. The converter is designed to function in continuous conduction mode irrespective of irradiance level variations. The connection diagram of the proposed Landsman converter is given in Fig. 3.

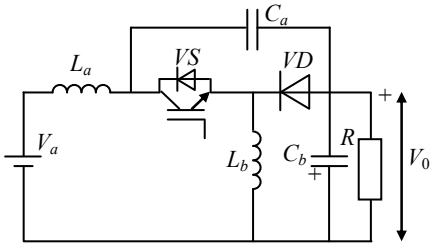

Fig. 3. Landsman converter

The input voltage is given by V_a and the output voltage is given by V_0. The switch is represented as VS and the output resistance is denoted as R. The current across the inductors L_a, L_b and the voltage across C_a are continuous in nature. It has the ability to boost the output and functions in boost mode when the value of duty ratio is greater than 50 %.

Operating mode 1 – switch ON. In operating mode 1, the switch is in ON condition and the voltage of capacitor

C_a termed as V_{Ca} reverse biases the diode. The current across L_b termed as I_{Lb} flows along the switch. Since V_{Ca} is greater than the resultant voltage V_0, and C_a discharges along the switch, transmitting energy to the inductor L_b and the output. Hence, V_{Ca} decreases and I_{Lb} increases and the input supplies energy to the input inductor L_a.

Operating mode 2 – switch OFF. In operating mode 2, the switch is in OFF condition and the forward biasing of diode results in a configuration of circuit as given in Fig. 3. The current across inductor L_b termed as I_{Lb} flows along the diode VD. The inductor L_b transmits its energy retained to output across the diode. Consequently, C_a is charged across the diode with the energy from both the input as well as L_a and hence, V_{Ca} increases while I_{Lb} decreases.

The ripple in the input current I_{La} is calculated by considering the flow of all the ripple component of L_a across C_a. $\Delta\phi$ represents the additional flux and the peak-to-peak ripple current is given by:

$$\Delta I_{La} = \Delta\phi / L_a \,. \tag{8}$$

At switch off condition, the current across C_a is given as:

$$I_{Ca} = I_{La} = C_a \cdot \frac{\Delta V_{Ca}}{(1-D)\cdot t_s}, \tag{9}$$

where D is the duty ratio; t_s is the switching period.

The voltage ripple content of V_{Ca} is given as:

$$\Delta V_{Ca} = \frac{I_{La}}{C_a}\cdot(1-D)\cdot t_s \,. \tag{10}$$

Substitute (10) in (8):

$$\Delta I_{La} = \frac{1}{2}\cdot\frac{1}{L_a}\cdot\frac{I_{La}}{2\cdot C_a}\cdot(1-D)\cdot t_s\cdot\frac{t_s}{2} = \\ = \frac{1}{8\cdot L_a\cdot C_a}\cdot\frac{I_{La}\cdot(1-D)}{f_{sw}^2}, \tag{11}$$

where $f_{sw} = 1/t_s$ is the switching frequency.

Equation (11) is normalized as:

$$\frac{\Delta I_{La}}{I_{La}} = \frac{1}{8\cdot L_a\cdot C_a}\cdot\frac{(1-D)}{f_{sw}^2}. \tag{12}$$

So, we have:

$$I_{La} = \frac{D}{(1-D)}\cdot I_0 \,. \tag{13}$$

where I_0 is the current at the output side.

Substitute (13) in (11)

$$L_a = \frac{D\cdot I_0}{8\cdot f_{sw}^2\cdot C_a\cdot\Delta I_{La}} \,. \tag{14}$$

Modelling of MPPT controller. In «neuro-fuzzy» method different learning concepts from the neural network literature are applied to a FIS. Figure 4 shows the model of ANFIS and it possesses the merits of both neural network as well as fuzzy logic controllers. Comparing with existing techniques of MPPT, the ANFIS adopted MPPT controller offers improved accuracy for tracking with high convergence speed.

The three major components present in the ANFIS are a rule based one dealing with choosing fuzzy rules, a database concept representing the membership functions of fuzzy rules and a decision engine for depicting the output adopting inference procedure. Expert awareness

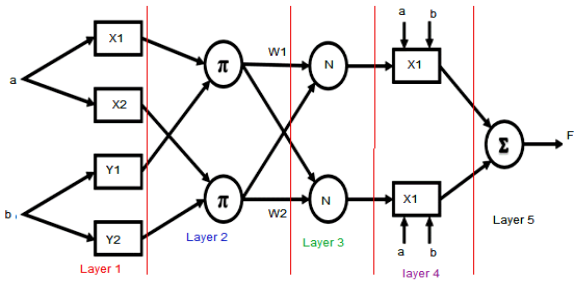

Fig. 4. Proposed ANFIS model

encompasses fuzzy logic principles, while neural network schemes are developed with the data base. Furthermore, the neuro-fuzzy approach appears to be appropriate if the system's data as well as information sources are available. In this approach, ANFIS based MPPT controller is utilized in PV system for tracking optimal power with minimal oscillation and the optimized fuzzy rules are attained by the embedding of the behavior of the complete system.

The outputs are obtained as the linear combination of the corresponding inputs and the fuzzy rules are given below:

1. When $a = X_1$, $b = Y_1$ then $F_1 = i_1 a + j_1 a + k_1$;
2. When $a = X_2$, $b = Y_2$ then $F_2 = i_2 a + j_2 a + k_2$;

Layer 1 comprises adaptive nodes capable of generating membership gradings of linguistic labels depending on assumed signals utilizing a proper parameterized membership function given as:

$$O_{1p} = \mu_{X_p}(a) = \frac{1}{1+\left|\dfrac{a-c_p}{x_p}\right|^{2\cdot y_p}}, \tag{15}$$

where O_{1p} represents the p^{th} node output of initial layer; a is the node input p; X_i is the linguistic label obtained from $X = (X_1, X_2, Y_1, Y_2)$ which represents the fuzzy set and $\{x_p, y_p, z_p\}$ represents the premise parameter set utilized for adjusting the membership function's shape.

Layer 2 comprises nodes which are fixed and designated as Π, further represented as the firing strength of every rule. The fuzzy AND of all inputs is taken as the output of every node:

$$O_{2p} = W_p = \mu_{X_p}(a)\cdot\mu_{Y_p}(b),\ p = 1,2,... \tag{16}$$

Layer 3 results are firing strengths which are normalized and the p^{th} node output is given by the ratio of the firing strength of p^{th} rule to the total of all rules of firing strengths:

$$O_{3p} = \overline{W_p} = \frac{W_p}{W_1 + W_2} \,. \tag{17}$$

Layer 4 outputs are calculated by the adaptive nodes depending on parameters utilizing:

$$O_{4p} = \overline{W_p}\cdot F_p = \overline{W_p}\cdot(i_p\cdot a + j_p\cdot b + k_p), \tag{18}$$

where $\overline{W_p}$ is the firing strength from the third layer and (i_p, y_p, k_p) are the nodes consequent parameter set.

Layer 5 estimates the overall output of ANFIS from the total of the inputs of nodes:

$$O_{5p} = \sum_{i=1}^{p}\overline{W_p}\cdot F_p = \frac{\sum_{i=1}^{p} W_p\cdot F_p}{\sum_{i=1}^{p} W_p} \,. \tag{19}$$

The current, power of the PV system and the duty cycle ratio of the converter are obtained as outputs by ANFIS controller. The input labels permit the ANFIS for generating the converter command which is further fed to the converter for ensuring power adaptation.

RNN based reference current generation. The increased usage of non-linear loads leads to distortions in current and voltage; however, there are several methods to mitigate harmonics. The injection of opposite harmonics in the PCC is one of the effective methods. For this, accurate reference current generation is necessary and this is accomplished in this work by RNN. The illustration of RNN is given in Fig. 5 and the process of harmonics extraction is in Fig. 6.

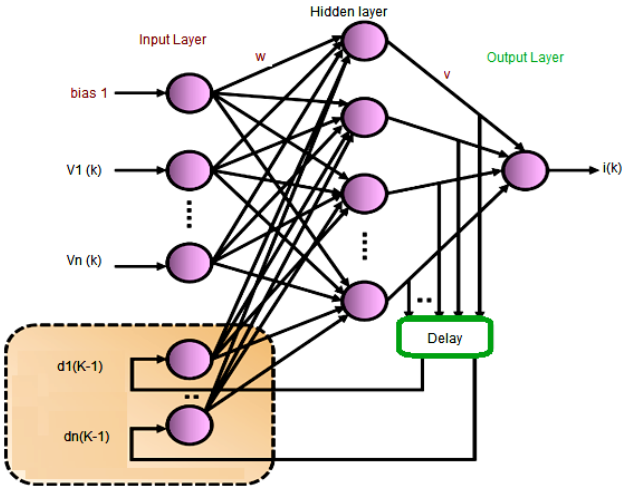

Fig. 5. Structure of RNN

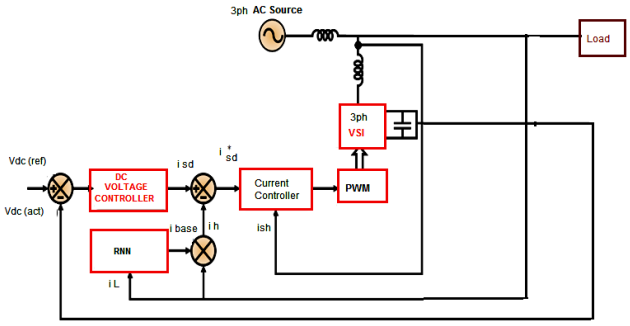

Fig. 6. Reference current generation

The structure of RNN resembles Elman network, in which the hidden layer's output at (k–1), is taken as the additional input for every sample step k. As the feedback is included from the prior step, an additional memory is included so that the neural network has the ability to grasp the dynamic behavior of the system. Back-propagation training is utilized for updating the weights.

By RNN, the harmonic components i_h is extracted from the load current i_L and the expression relating the harmonic component and load current is given as:

$$i_h = i_L - i_{base}, \tag{20}$$

where the fundamental component is denoted as i_{base}, the reference current i_{sd}^* is generated exactly by RNN thereby eliminating the harmonics.

RNN consists of numerous successive recurrent layers, and these layers are sequentially modeled in order to map the sequence with other sequences. RNN has a strong capability in order to capture the contextual data from the sequence. RNN can operate the sequences with arbitrary length. RNN is the extension of feed forward neural network with the presence of loops in hidden layers. RNN takes the input with the sequence of samples and identifies the time relationship between the samples. The LSTM solves the classification issues by adding the network parameters with the hidden node and releases the state based on the input values. RNN achieves better performance than LSTM by activating the states based on network events. The regular RNN node consists of a single bias and weight. The RNN is evaluated using the gated recurrent unit and LSTM. The one-to-one network configuration is formed using the network parameters, where the time step of each input data generates the output with the specific time step.

- Forget gate layer;
- Input gate layer;
- Output gate layer;
- State gate layer.

The input and the forget gate controls the previous hidden state and the present input state that contributes to the cells state. However, the input, output, and the forget gate activation is scaled using the sigmoid function, and the output of the hidden state is filtered using the hyperbolic function. The optimization of network parameters using the stochastic gradient is achieved based on the sequence of input data. However, the hyperparameters are the structure of the network (size and layers), sequence length, batch size, momentum, and learning rate, respectively. The hyperparameters are set through the stochastic or manual search.

The input of the RNN is the sequence of vectors as $\{y_1, y_2, ..., y_M\}$ the sequence of hidden states as $\{z_1, z_2, ..., z_M\}$ and the output unit as $\{v_1, v_2, ..., v_M\}$ respectively.

The recurrent layer consists of the recurrent function d, which takes the input vector yx and the hidden unit of the previous state zx as the input and generates the hidden state as:

$$zx = d(yx, zx-1) = \tanh(P \cdot yx + Q \cdot zx - 1). \tag{21}$$

Moreover, the output units are calculated as:

$$vx = \text{soft}\max(R \cdot zx), \tag{22}$$

where P, Q, R are the weight matrices; and the activation function tanh indicates the hyperbolic tangent function.

RNN uses the highly complicated function in order to learn and control the information flow in the recurrent layer for capturing the long term dependencies.

Results and discussions. The analysis of PV fed STATCOM assisting harmonics elimination, providing voltage stability is validated through MATLAB environment in this work. The output voltage of the PV system has been enhanced by exploiting the Landsman converter, through which the performance of the system is improved. The DC-link voltage stability is regulated through the ANFIS adopted MPPT controller offering high accuracy with increased speed of convergence. The specifications of PV module and Landsman converter are illustrated in Table 1.

The proposed work is implemented in MATLAB depicted in Fig. 7 and the obtained results are given below.

Table 1

Specifications PV module and Landsman converter

Parameter name	Value
Cells in a module	36
Modules in series	17
Modules in parallel	4
Open circuit voltage V_{oc}, V	21
Short circuit current I_{sc}, A	7.1
Converter duty ratio D	0.5
Capacitance C_a, μF	4.7
Capacitance C_b, μF	1000
Inductance L_a, mH	0.9
Inductance L_b, mH	5.4
Capacitance C_f, μF	650
Resistance R_c, Ω	0.03
Inductance L_f, mH	0.7
Resistance R_f, Ω	0.01

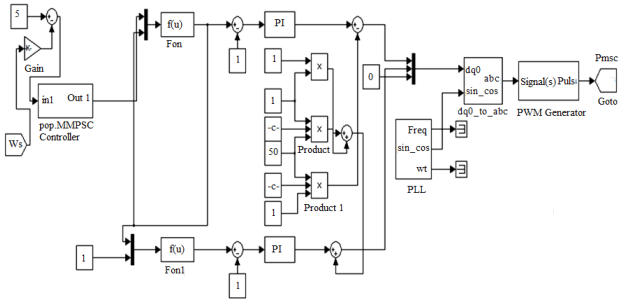

Fig. 7.Control block of RNN

Figure 8 indicates the waveform for solar irradiation. Its increase leads to the increase of output current as well as voltage. This results in maximum power output in this mode of operation.

Figure 9 indicates the waveform for temperature. The increase in operating temperature results in the marginal increase of output current, but leads to decrease in output voltage and hence results in the decrease of net output power.

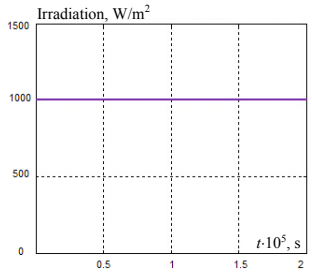

Fig. 8. Waveform for solar irradiation

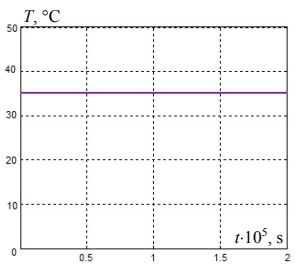

Fig. 9. Waveform for temperature

Figures 10, 11 denote the waveforms for output voltage and output current in PV panel respectively. The output voltage obtained is a constant DC voltage with varying time.

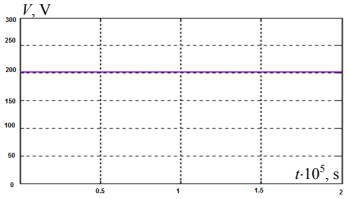

Fig. 10. Output voltage waveform for PV panel

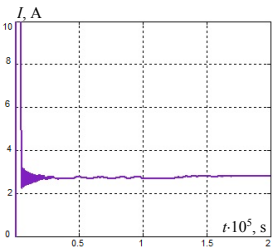

Fig. 11. Output current waveform for PV panel

Figures 12, 13 denote the output voltage waveform as well as output current waveform for a switched boost Landsman converter. The adopted ANFIS based MPPT extracts maximum power from the PV panel and is fed to the converter which further minimizes the ripples.

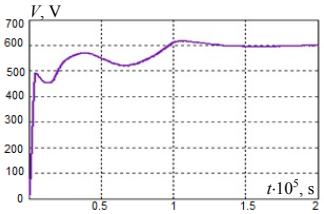

Fig. 12. Output voltage waveform for switched boost Landsman converter

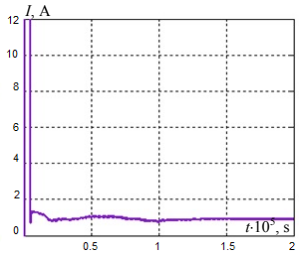

Fig. 13. Output current waveform for switched boost Landsman converter

Figure 14 denotes the AC output voltage waveform for VSI with varying magnitude and frequency. The comparison of reference signal is performed with a carrier waveform of increased frequency for controlling the inverter's AC output voltage.

Figure 15 indicates the output voltage waveform for grid which is sinusoidal in nature with constant voltage and frequency.

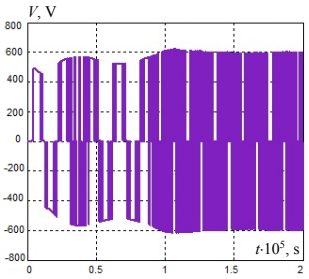

Fig. 14. Output voltage waveform for VSI

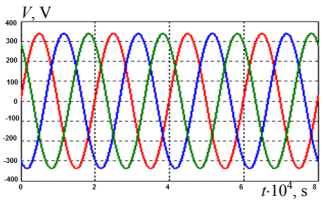

Fig. 15. Output voltage waveform for grid

Figure 16 indicates the output current waveform for grid which is sinusoidal in shape during its operation maintaining constant voltage and frequency. The grid current THD (Fig. 17) has been observed as 3.5 %, which satisfies the IEEE standard.

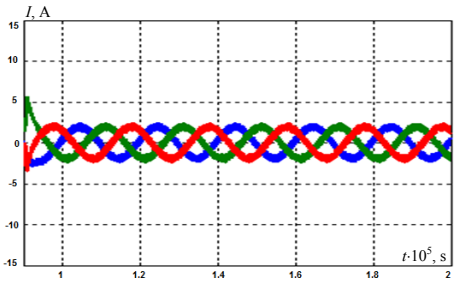

Fig. 16. Output current waveform for grid

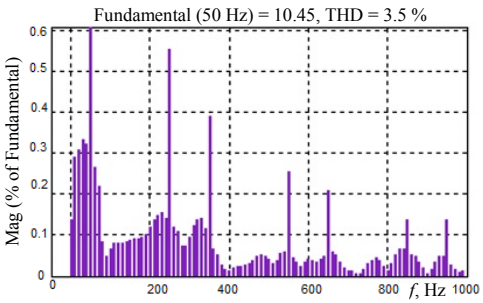

Fig. 17. Grid current THD

The performance of the converter is analyzed in terms of its efficiency and voltage gain ratio. In both the aspects the proposed Landsman converter provides better results as shown in Fig. 18, with a maximum efficiency of 92 % and gain of 10.

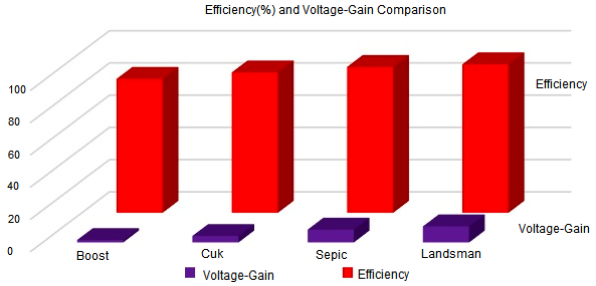

Fig. 18. Comparison of efficiency and voltage-gain for Landsman converter

The tracking efficiency of the proposed MPPT algorithm is revealed to be more effective when analogized with conventional algorithms like P-O, IC and fuzzy. The tracking efficiency (Fig. 19) of P-O algorithm, IC, fuzzy and ANFIS are observed as 81 %, 84 %, 89 % and 92 % respectively.

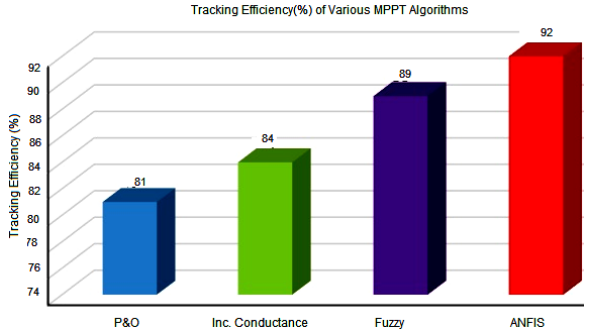

Fig. 19. Comparison of tracking efficiency

DC-link voltage control plays a key role in determining the overall performance of the system, by which the voltage stability is ensured. Better settling time and THD is accomplished by using the proposed RNN based reference current generation whereas the PI controller and SRF theory delivers relatively low values depicted in Table 2.

Table 2

Comparison of settling time and THD

	PI	SRF	RNN
Settling time, $s \cdot 10^{-5}$	3.2	2.7	1.75
THD	4.7 %	4.2 %	3.5 %

Experimental setup. The PV array integrated utility grid using high gain converters hardware setup shown in Fig. 20. The operation of the STATCOM under two different cases.

Method 1. In this method the outer loop and inner loop of the grid used is PI voltage regulator and PI current controller.

Method 2. In the method the outer voltage loop used in PI voltage regulator and inner current loop used as RNN current controller. The above different methods to assure the controller performance at different system parameters, the local loads on grid side and solar irradiance has been changed as follows:

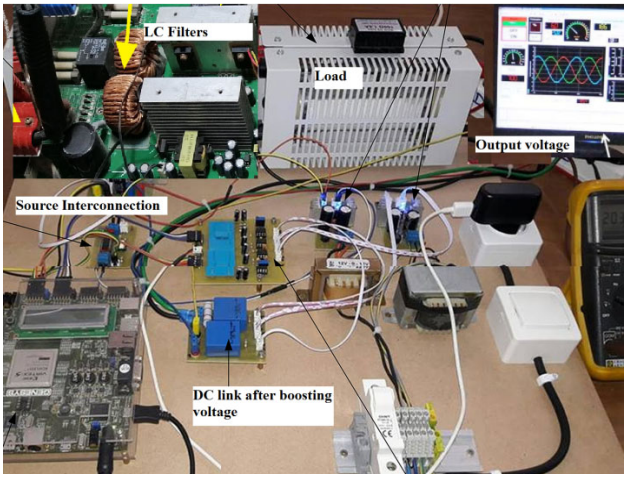

Fig. 20. Hardware setup for grid connected solar PV systems using STATCOM

1. Without any break 10 kW inductive load is applied and 0.8 s with 5 kW one more inductive load is applied.

2. Duration of 0.4 s to 0.6 s solar irradiance is changed from 1000 W/m^2 to 600 W/m^2.

In hardware circuit, displays the voltage and current before the boost converter of PV terminal. The current is changed with respect to change in irradiance of the solar PV panel. The PV array voltage level is changed by using high gain.

The proposed RNN controller shows better harmonic reduction than existing PI current controller. Moreover, the voltage stability of the system maintain with solar PV interconnected with distribution grid even under dynamic changes.

The load current of solar interconnected PV system is shown in Fig. 21.

For various operating condition the single stage grid connected system was studied and the off mode grid with solar PV system for disconnected source voltage depicted in Fig. 22.

The isolation condition of 1000 W/m^2 is 400 V PV model power for reactive power by the inverter output shown in Fig. 23.

In this case the isolation level on the PV panel was varied as shown in the Fig. 24.

The FFT analysis of output voltage for the grid interconnected THD is depicted in Fig. 25 and the reduced THD is 4.24 %.

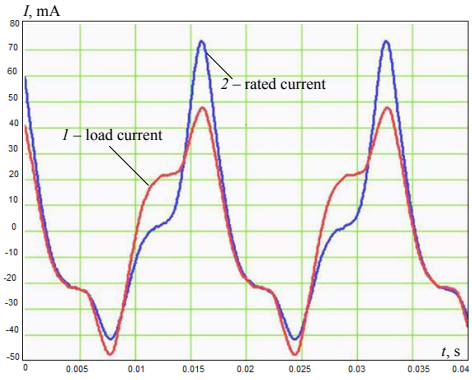

Fig. 21. Load current

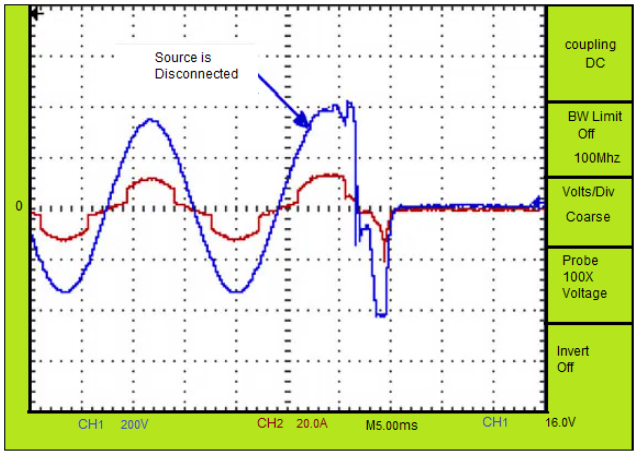

Fig. 22. Disconnected source voltage

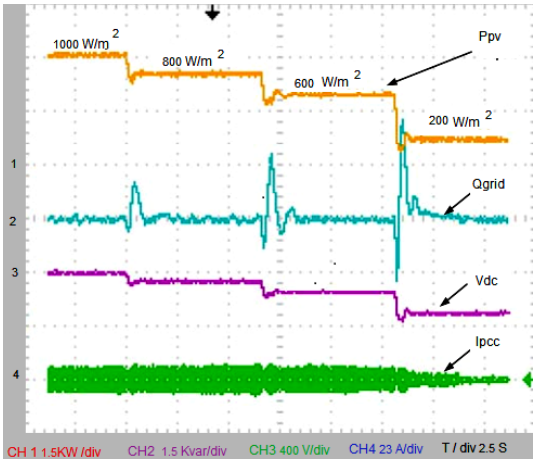

Fig. 23. PV module power P_{pv}, reactive power Q_{grid} supplied by inverter, DC link voltage V_{dc}, current at the PCC I_{pcc} for variable isolation

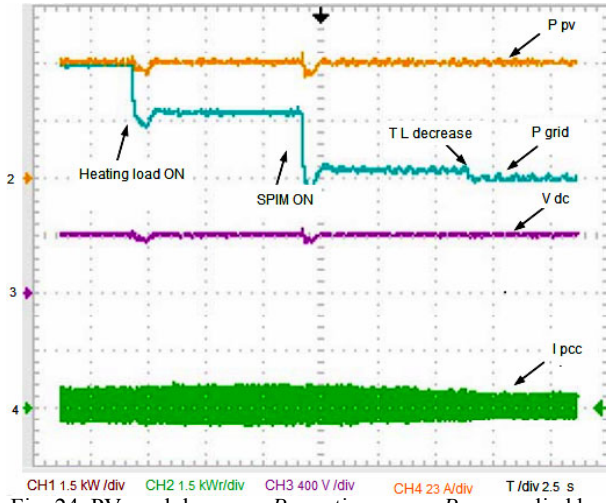

Fig. 24. PV module power P_{pv}, active power P_{grid} supplied by inverter, DC link voltage V_{dc}, current at the PCC I_{pcc} for switching ON of local load

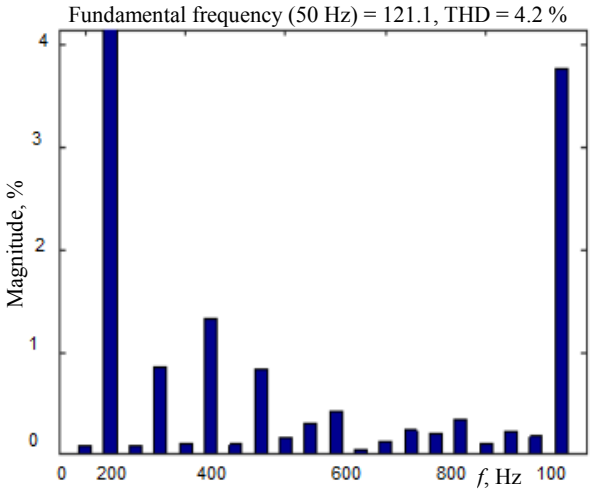

Fig. 25. The performance of FFT analysis of output voltage for THD

The observation.

1. The proposed model, active power, reactive power injected for different isolation level, the inverter DC link voltage and current fed to the grid.
2. The THD level of the current is found to be below 5 %.
3. The reactive power is maintained at zero level in order to ensure the unity power factor operation.
4. Reactive power injected by the system voltage regulation at the terminal of the inverter the can be adjusted.
5. The system for a strong interconnection grid system, the performance of the controller is much better and faster as compared to that for a weak interconnected grid system.

While implementing the practical consequences, there will be a ripple current significant rise whenever the inverter feeds non-linear load, and its majority of concern is magnetizing current. The hardware prototype sampling time, harmonics will be slightly higher than its simulation results. It can be suppressed by either increasing the number of levels of inverter or designing a filter.

Conclusions.

In this paper, an efficient way of regulating voltage stability and mitigating harmonics is addressed by using a photovoltaic fed static synchronous compensator with recurrent neural network. Static synchronous compensator is basically shunt connected, which provides reactive power compensation and voltage stability. DC-DC converters has been incorporated with photovoltaic systems and Landsman converter has been utilized in this work along with adaptive neuro-fuzzy inference system maximum power point tracking for tracking the maximum power from the photovoltaic, along with DC-link voltage regulation. The chosen converter provides better efficiency and voltage-gain ratio when compared with other converters. Recurrent neural network assists in the generation of reference signal, so that the harmonics that occur in the system are effectively mitigated. The validation of the proposed work is carried out through simulation in MATLAB and also tested with hardware model. It has been observed that the total harmonic distortions is minimized to 5 % which suits IEEE standard.

Conflict of interest. The authors declare that they have no conflicts of interest.

REFERENCES

1. Chowdhury B.H. Optimizing the integration of photovoltaic systems with electric utilities. *IEEE Transactions on Energy Conversion*, 1992, vol. 7, no. 1, pp. 72-78. doi: https://doi.org/10.1109/60.124544.

2. Yazdani A., Dash P.P. A Control Methodology and Characterization of Dynamics for a Photovoltaic (PV) System Interfaced With a Distribution Network. *IEEE Transactions on Power Delivery*, 2009, vol. 24, no. 3, pp. 1538-1551. doi: https://doi.org/10.1109/TPWRD.2009.2016632.

3. Babu V., Ahmed K.S., Shuaib Y.M., Manikandan M. Power Quality Enhancement Using Dynamic Voltage Restorer (DVR)-Based Predictive Space Vector Transformation (PSVT) With Proportional Resonant (PR)-Controller. *IEEE Access*, 2021, vol. 9, pp. 155380-155392. doi: https://doi.org/10.1109/ACCESS.2021.3129096.

4. Babu V., Ahmed K.S., Shuaib Y.M., Mani M. A novel intrinsic space vector transformation based solar fed dynamic voltage restorer for power quality improvement in distribution system. *Journal of Ambient Intelligence and Humanized Computing*. 2021. doi: https://doi.org/10.1007/s12652-020-02831-0.
5. Li C., Burgos R., Wen B., Tang Y., Boroyevich D. Stability Analysis of Power Systems With Multiple STATCOMs in Close Proximity. *IEEE Transactions on Power Electronics*, 2020, vol. 35, no. 3, pp. 2268-2283. doi: https://doi.org/10.1109/TPEL.2019.2931891.
6. Hou X., Sun Y., Han H., Liu Z., Su M., Wang B., Zhang X. A General Decentralized Control Scheme for Medium-/High-Voltage Cascaded STATCOM. *IEEE Transactions on Power Systems*, 2018, vol. 33, no. 6, pp. 7296-7300. doi: https://doi.org/10.1109/TPWRS.2018.2865127.
7. Kumar N., Singh B., Panigrahi B.K., Xu L. Leaky-Least-Logarithmic-Absolute-Difference-Based Control Algorithm and Learning-Based InC MPPT Technique for Grid-Integrated PV System. *IEEE Transactions on Industrial Electronics*, 2019, vol. 66, no. 11, pp. 9003-9012. doi: https://doi.org/10.1109/TIE.2018.2890497.
8. Anand I., Senthilkumar S., Biswas D., Kaliamoorthy M. Dynamic Power Management System Employing a Single-Stage Power Converter for Standalone Solar PV Applications. *IEEE Transactions on Power Electronics*, 2018, vol. 33, no. 12, pp. 10352-10362. doi: https://doi.org/10.1109/TPEL.2018.2804658.
9. Li R., Shi F. Control and Optimization of Residential Photovoltaic Power Generation System With High Efficiency Isolated Bidirectional DC–DC Converter. *IEEE Access*, 2019, vol. 7, pp. 116107-116122. doi: https://doi.org/10.1109/ACCESS.2019.2935344.
10. Babu V., Basha S.S., Shuaib Y.M., Manikandan M., Enayathali S.S. A novel integration of solar fed dynamic voltage restorer for compensating sag and swell voltage in distribution system using enhanced space vector pulse width modulation (ESVPWM). *Universal Journal of Electrical and Electronic Engineering*, 2019, vol. 6, no. 5, pp. 329-350. doi: https://doi.org/10.13189/ujeee.2019.060504.
11. Ahmad M.W., Gorla N.B.Y., Malik H., Panda S.K. A Fault Diagnosis and Postfault Reconfiguration Scheme for Interleaved Boost Converter in PV-Based System. *IEEE Transactions on Power Electronics*, 2021, vol. 36, no. 4, pp. 3769-3780. doi: https://doi.org/10.1109/TPEL.2020.3018540.
12. Chandrasekar B., Nallaperumal C., Padmanaban S., Bhaskar M.S., Holm-Nielsen J.B., Leonowicz Z., Masebinu S.O. Non-Isolated High-Gain Triple Port DC–DC Buck-Boost Converter With Positive Output Voltage for Photovoltaic Applications *IEEE Access*, 2020, vol. 8, pp. 113649-113666. doi: https://doi.org/10.1109/ACCESS.2020.3003192.
13. Huang Q., Huang A.Q., Yu R., Liu P., Yu W. High-Efficiency and High-Density Single-Phase Dual-Mode Cascaded Buck–Boost Multilevel Transformerless PV Inverter With GaN AC Switches. *IEEE Transactions on Power Electronics*, 2019, vol. 34, no. 8, pp. 7474-7488. doi: https://doi.org/10.1109/TPEL.2018.2878586.
14. Andrade A.M.S.S., Schuch L., da Silva Martins M.L. High Step-Up PV Module Integrated Converter for PV Energy Harvest in FREEDM Systems. *IEEE Transactions on Industry Applications*, 2017, vol. 53, no. 2, pp. 1138-1148. doi: https://doi.org/10.1109/TIA.2016.2621110.
15. Padmanaban S., Priyadarshi N., Bhaskar M.S., Holm-Nielsen J.B., Hossain E., Azam F. A Hybrid Photovoltaic-Fuel Cell for Grid Integration With Jaya-Based Maximum Power Point Tracking: Experimental Performance Evaluation. *IEEE Access*, 2019, vol. 7, pp. 82978-82990. doi: https://doi.org/10.1109/ACCESS.2019.2924264.
16. Han B., Lai J.-S., Kim M. Dynamic Modeling and Controller Design of Dual-Mode Cuk Inverter in Grid-Connected PV/TE Applications. *IEEE Transactions on Power Electronics*, 2018, vol. 33, no. 10, pp. 8887-8904. doi: https://doi.org/10.1109/TPEL.2017.2779843.
17. Manikandan M., Basha A.M. ODFF: Optimized Dual Fuzzy Flow Controller Based Voltage Sag Compensation for SMES-Based DVR in Power Quality Applications. *Circuits and Systems*, 2016, vol. 7, no. 10, pp. 2959-2974. doi: https://doi.org/10.4236/cs.2016.710254.
18. Moradi-Shahrbabak Z., Tabesh A. Effects of Front-End Converter and DC-Link of a Utility-Scale PV Energy System on Dynamic Stability of a Power System. *IEEE Transactions on Industrial Electronics*, 2018, vol. 65, no. 1, pp. 403-411. doi: https://doi.org/10.1109/TIE.2017.2721902.
19. Venkatramanan D., John V. Dynamic Modeling and Analysis of Buck Converter based Solar PV Charge Controller for Improved MPPT Performance. *2018 IEEE International Conference on Power Electronics, Drives and Energy Systems (PEDES)*, 2018, pp. 1-6, doi: https://doi.org/10.1109/PEDES.2018.8707505.
20. Zhou Y., Ho C.N.M., Siu K.K.-M. A Fast PV MPPT Scheme Using Boundary Control With Second-Order Switching Surface. *IEEE Journal of Photovoltaics*, 2019, vol. 9, no. 3, pp. 849-857. doi: https://doi.org/10.1109/JPHOTOV.2019.2899470.
21. Bana P.R., Panda K.P., Padmanaban S., Mihet-Popa L., Panda G., Wu J. Closed-Loop Control and Performance Evaluation of Reduced Part Count Multilevel Inverter Interfacing Grid-Connected PV System. *IEEE Access*, 2020, vol. 8, pp. 75691-75701. doi: https://doi.org/10.1109/ACCESS.2020.2987620.
22. Li F., Qin J., Kang Y. Closed-Loop Hierarchical Operation for Optimal Unit Commitment and Dispatch in Microgrids: A Hybrid System Approach. *IEEE Transactions on Power Systems*, 2020, vol. 35, no. 1, pp. 516-526. doi: https://doi.org/10.1109/TPWRS.2019.2931293.
23. Cantillo A., De Nardo A., Femia N., Zamboni W. Stability Issues in Peak-Current-Controlled SEPIC. *IEEE Transactions on Power Electronics*, 2011, vol. 26, no. 2, pp. 551-562. doi: https://doi.org/10.1109/TPEL.2010.2066288.
24. Swain S., Subudhi B. Grid Synchronization of a PV System With Power Quality Disturbances Using Unscented Kalman Filtering. *IEEE Transactions on Sustainable Energy*, 2019, vol. 10, no. 3, pp. 1240-1247. doi: https://doi.org/10.1109/TSTE.2018.2864822.
25. Kewat S., Singh B. Grid Synchronization of WEC-PV-BES Based Distributed Generation System Using Robust Control Strategy. *IEEE Transactions on Industry Applications*, 2020, vol. 56, no. 6, pp. 7088-7098. doi: https://doi.org/10.1109/TIA.2020.3021060.
26. Abdul R.A. Solar PV System for Water Pumping Incorporating an MPPT based Bat Optimization Circuits and Systems. *Journal of Advanced Research in Dynamical and Control Systems*, 2020, vol. 12, no. 01-Special Issue, pp. 786-794. doi: https://doi.org/10.5373/JARDCS/V12SP1/20201130.
27. Moyo R.T., Tabakov P.Y., Moyo S. Design and Modeling of the ANFIS-Based MPPT Controller for a Solar Photovoltaic System. *Journal of Solar Energy Engineering*, 2021, vol. 143, no. 4, p. 041002. doi: https://doi.org/10.1115/1.4048882.
28. Grossi E., Buscema M. Introduction to artificial neural networks. *European Journal of Gastroenterology & Hepatology*, 2007, vol. 19, no. 12, pp. 1046-1054. doi: https://doi.org/10.1097/MEG.0b013e3282f198a0.
29. Kalaiarasi N., Nagalakshmaiah E., Dash S.S., Paramasivam S. Development and analysis of ANN based MPPT and SL Z-source inverter for photovoltaic systems. *International Journal of Control Theory and Applications*, 2016, vol. 9, no. 39, pp. 313-323. Available at: https://serialsjournals.com/abstract/39638_cha-36.pdf (Accessed 11 May August 2021).

Received 25.12.2021
Accepted 12.02.2022
Published 20.04.2022

Thota Praveen Kumar[1], *Research Scholar,*
Somaskandan Ganapathy[1], *Professor,*
Mani Manikandan[2], *Professor,*
[1] Annamalai University,
Chidambaram, Tamil Nadu, 608002, India,
e-mail: thotap@rediffmail.com (Corresponding author),
ganapathy1967@gmail.com
[2] Jyothishmathi Institute of Technology and Science,
Karimnagar, Telangana, 505481, India,
e-mail: cm.manikandan@gmail.com

How to cite this article:
Praveen Kumar T., Ganapathy S., Manikandan M. Improvement of voltage stability for grid connected solar photovoltaic systems using static synchronous compensator with recurrent neural network. *Electrical Engineering & Electromechanics*, 2022, no. 2, pp. 69-77. doi: https://doi.org/10.20998/2074-272X.2022.2.10